Rapid Communications

# Spatiotemporal intermittency and localized dynamic fluctuations upon approaching the glass transition

J. Ariel Rodriguez Fris,[1] Eric R. Weeks,[2] Francesco Sciortino,[3,4] and Gustavo A. Appignanesi[1]

[1]*INQUISUR, Departamento de Química, Universidad Nacional del Sur (UNS)-CONICET, Avenida Alem 1253, 8000 Bahía Blanca, Argentina*

[2]*Physics Department, Emory University, Atlanta, Georgia 30322, USA*

[3]*Dipartimento di Fisica, Sapienza Universita' di Roma, Piazzale A. Moro 5, Roma 00185, Italy*

[4]*CNR-ISC, c/o Sapienza, Piazzale A. Moro 5, Roma 00185, Italy*

(Received 5 January 2018; published 25 June 2018)

We introduce a robust approach for characterizing spatially and temporally heterogeneous behavior within a system based on the evolution of dynamic fluctuations averaged over different space lengths and timescales. We apply it to investigate the dynamics in two canonical systems as the glass transition is approached: simulated Lennard-Jones liquids and experimental dense colloidal suspensions. In both cases the onset of glassiness is marked by spatially localized dynamic fluctuations originating in regions of correlated mobile particles. By removing the trivial system size dependence we show that the spatial heterogeneity of the dynamics extends to large length scales containing tens to hundreds of particles, corresponding to the timescale of maximally non-Gaussian dynamics.

DOI: 10.1103/PhysRevE.97.060601

Glasses are solid materials with disordered liquidlike structure. These are typically formed by rapidly quenching a liquid from a hot to a cold temperature, or compressing a liquid from a low to a high pressure [1,2]. How the transition from an equilibrium liquid to an out-of-equilibrium glass takes places is highly debated, with many different and contrasting interpretations proposed (see Refs. [3–9] for reviews). One point is known: the onset of unusual behavior within a sample precedes the glass transition. "Supercooled liquids," despite their metastable equilibrium, have a markedly higher viscosity $\eta$ than normal liquids. This steep rise of $\eta$ is associated with the onset of dynamical heterogeneity: diffusive motion takes place in a spatially and temporally heterogeneous fashion [10–14]. At any given time, some regions within the sample are frozen, while other regions are quite mobile. The mobile regions are characterized by "cooperative" motion where localized groups of molecules have nearly simultaneous large displacements [12,15–17]. Over time, the locations of faster and slower dynamics change, such that at any given position the dynamics are temporally heterogeneous as well [4,18,19]. It has been also found that the dynamics is most heterogeneous at a timescale $\Delta t^*$, the timescale that maximizes the non-Gaussian parameter $\alpha_2$ [20], which quantifies the measured frequency of large displacements as compared to a Gaussian distribution of displacements [15–17,21,22]. Identifying the particles responsible for the large $\alpha_2$ value is expected to provide information on the cooperatively moving clusters [15–17] and their structural and dynamic properties. Early studies [15–17] used various somewhat arbitrary criteria to define mobile particles. Later work examined spatial correlation functions averaged over all particles in various ways attempting to identify the length and timescales of dynamical heterogeneity [12,17,23–30].

In this Rapid Communication, we present a robust analysis method to characterize spatial and temporal dynamical heterogeneity that does not require any *a priori* definition of particle mobility. Our parameter-free method contrasts the spatial and temporal motion of particles with motion of a system in which motion is homogeneous in space and time and identical to that of the entire system. The system mean-square displacement thus acts as a "null hypothesis" for particle motion and we quantify deviations away from this null hypothesis. We apply this method to two archetypical glass-former systems: simulations of the Kob-Andersen mixture [31] and confocal microscopy data on colloidal suspensions [32]. Our results show that dynamical heterogeneity is most obvious for subsystems comprised of tens to hundreds of particles, with the size growing as the glass transition is approached. Additionally, we examine how dynamical heterogeneity becomes averaged out at larger length scales, finding that spatial variability of the dynamics persists to surprisingly large scales. As a by-product we confirm that $\Delta t^*$ is the timescale of maximum heterogeneity. While our method of localized fluctuations is applied to particle displacements, the idea is generalizable to other quantities which may have spatiotemporal fluctuations such as structure [33,34].

We use LAMMPS to simulate the Kob-Andersen binary Lennard-Jones (LJ) glass-forming system [31], an 80:20 mixture of $A$ and $B$ particles. The particles interact via the Lennard-Jones potential

$$U_{\alpha\beta}(r) = 4\epsilon_{\alpha\beta}\left[\left(\frac{\sigma_{\alpha\beta}}{r}\right)^{12} - \left(\frac{\sigma_{\alpha\beta}}{r}\right)^{6}\right] \tag{1}$$

with $\alpha,\beta \in A,B$. $A$ and $B$ particles have the same mass. The energy scales are $\epsilon_{AA} = 1.0$, $\epsilon_{AB} = 1.5$, and $\epsilon_{BB} = 0.5$. The size scales are $\sigma_{AA} = 1.0$, $\sigma_{AB} = 0.8$, and $\sigma_{BB} = 0.88$, chosen so that $A$ and $B$ particles are encouraged to mix rather than segregate, and thus crystallization is frustrated [31]. For most of our results we present data with 8000 total particles, and for our analysis we consider the $N = 6400$ $A$ particles. To verify

 

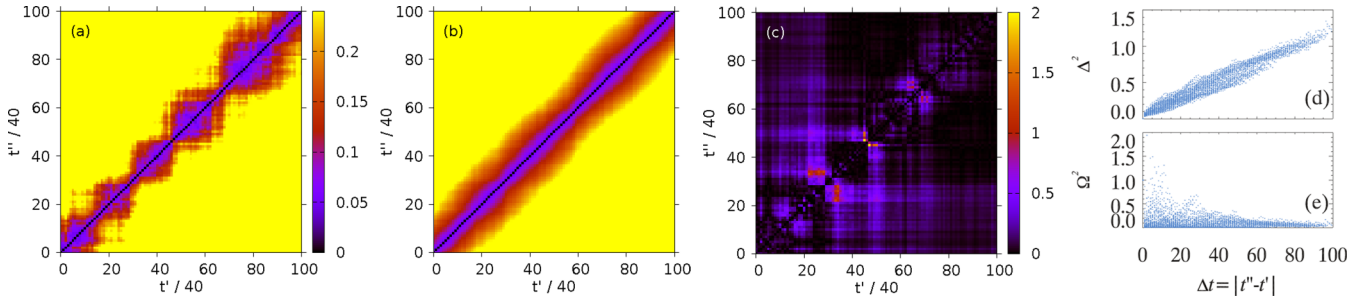


FIG. 1. (a) Contour plot of the distance matrix $\Delta^2(t',t'')$ for a binary Lennard-Jones system at $T = 0.50$ within a cubical subsystem containing 125 particles. (b) Contour plot of the same system for the full 8000 particle simulation. Data taken from Ref. [29]. (c) $\Omega(t',t'')$. The data correspond to the same subsystem as in (a). In the image shown, darker points indicate smaller values. (d) The values of $\Delta^2$ as a function of $\Delta t = |t' - t''|$ for the data shown in (a). For small $\Delta t$ this tends to 0, and for intermediate $\Delta t$ the scatter indicates the temporal heterogeneity in this subsystem. The overall increase mirrors the mean-square displacement $M^2(\Delta t)$. (e) $\Omega^2(\Delta t)$ for the data shown in (c). The scatter at small $\Delta t$ reflects the non-Gaussian statistics of the displacements at those time scales.

that our analysis is not biased by finite size, in a few cases we compare with a $N = 8\times10^5$ data set. Periodic boundary conditions were used with a cubical box.

In turn, we reanalyze previously published data from experiments using confocal microscopy to observe dense colloidal samples [32]. The samples were sterically stabilized colloidal poly-(methyl methacrylate) for which the key control parameter is the volume fraction $\phi$. The glass transition for this experiment occurred at $\phi_g = 0.58$. Here we examine data with $\phi = 0.46, 0.52, 0.56$ with $N \approx 2500, 2900, 3100$ particles, respectively, in the observation volume. The particles were a single species with mean particle diameter 2.36 $\mu$m and a polydispersity of 0.045 and were slightly charged. Confocal microscopy and particle tracking was used to follow the positions of the particles in three dimensions. The imaging volume was rectangular with an aspect ratio roughly 5:5:1 (see Ref. [32] for details).

We aim at characterizing the growing spatial and temporal fluctuations on approaching the glass transition without introducing any arbitrary cut-off quantity. Following prior work [28,29,35], we start by defining the distance matrix $\Delta^2(t',t'')$, an object that represents the average of the squared particle displacements between particular times $t'$ and $t''$ of a collection of the $N$ particles belonging to a predefined set $S$ ($S$ may be the entire system or some subsystem):

$$\Delta^2(t',t'') \equiv \frac{1}{N}\sum_{i=1}^{N} |\vec{r}_i(t') - \vec{r}_i(t'')|^2 \tag{2}$$

$$= \langle |\vec{r}_i(t') - \vec{r}_i(t'')|^2 \rangle_{i\in S}, \tag{3}$$

where the angle brackets indicate an average over the $N$ particles in $S$. Further averaging $\Delta^2(t',t'')$ over all pairs $t'$ and $t''$ such that $t'' - t' = \Delta t$ produces the well-known average mean-square displacement $M^2(\Delta t)$ of particles in $S$. More precisely, $M^2(\Delta t) = \langle \Delta^2(t',t'') \rangle_{t''-t'=\Delta t}$, where the average is over $t',t''$ with fixed time interval $\Delta t = |t'' - t'|$ and also over all of the particles in $S$. Assuming stationary dynamics (true as long as the system is not aging), for a sufficiently large $\Delta t$, $\lim_{\Delta t\to\infty} \Delta^2(t',t' + \Delta t) = M^2(\Delta t)$.

For small systems under glassy relaxation conditions, $\Delta^2$ has temporal fluctuations, as shown in Fig. 1(a) for a subsystem of $N = 125$ particles from a larger Lennard-Jones simulation. Darker regions indicate time intervals $(t',t'')$ over which this subsystem has relatively little particle motion. Clearly, there are specific times for which this subsystem undergoes fairly large changes, signaled by larger displacements. It is expected [36] that at any given time, different regions of the system are independent when sufficiently far apart. This implies that on increasing the subsystem size well beyond any dynamic correlation length, $\Delta^2$ will appear much smoother, as shown in Fig. 1(b) for the full system of $N = 8000$ particles. For a sufficiently large system $S$, the spatial fluctuations must average out such that $\lim_{N\to\infty} \Delta^2(t',t' + \Delta t) = M^2(\Delta t)$.

The question we turn to is how the large system limit is reached, and how this relates to the spatial scale of dynamical heterogeneities. Our approach of comparing specific sized subsystems is similar in spirit to Refs. [37,38] which used the $\chi_4$ analysis applied to subsystems. We wish to use the approach to the large system limit to characterize the spatial scale of dynamical heterogeneities. The obvious features of Fig. 1(a) are the large fluctuations that differentiate it from Fig. 1(b). This motivates us to consider the normalized difference between $\Delta^2$ and the expectation for a large system, defined by

$$\Omega^2_S(t',t'') = \frac{[\Delta^2(t',t'') - M^2(\Delta t)]^2}{[M^2(\Delta t)]^2} \tag{4}$$

with the convention $\Delta t = |t'' - t'|$. $\Omega^2_S$, a measure of dynamic intermittency, represents the matrix of normalized squared deviations from the mean value for the particles squared displacements and will be equal to zero when $\Delta^2$ is calculated for sufficiently large systems, for which time averages and space averages are equivalent and $\Delta^2 = M^2$. Otherwise, $\Omega^2_S > 0$ and larger values indicate larger deviations between $\Delta^2$ (local in both space and time) and the expectation for a large system (i.e., $M^2$, a quantity averaged over all space and all time).

An example of $\Omega^2_S(t',t'')$ is shown in Fig. 1(c), where the brighter regions indicate time periods for which the mean motion within the subvolume is anomalously larger or smaller compared to the expectation from $M^2$. Figures 1(d) and 1(e) show scatter plots of the values of $\Delta^2$ and $\Omega^2_S$ as functions of $t'' - t'$, taken from the data of Figs. 1(a) and 1(c), respectively. $\Delta^2$ starts at the origin and rises, consistent with the idea

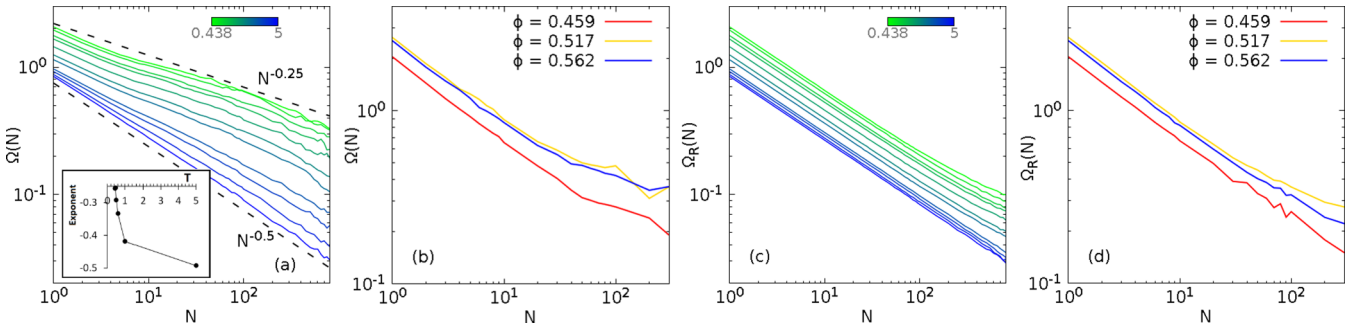


FIG. 2. $\Omega(N)$ and $\Omega_R(N)$ as a function of subsystem size $N$ for the binary Lennard-Jones system [(a) and (c)] for different temperatures as indicated and for the experimental colloidal suspension [(b) and (d)] at different volume fractions $\phi$ as indicated. In the case of $\Omega(N)$ the $N$ particles are part of the same subsystem. In the case of $\Omega_R(N)$ the $N$ particles are selected *randomly* among all particles in the system. The dashed lines in (a) indicate power-law decay with the exponents shown, and the inset to (a) shows the decay exponent as a function of $T$ for the data. The decay exponent is found by fitting the data for $N \leqslant 800$, and for all $T$ we find a high-quality fit ($R^2 \geqslant 0.99$).

that on average it should behave similar to the mean-square displacement $M^2(\Delta t)$. At intermediate timescales the scatter in the data of Fig. 1(d) indicates the temporal fluctuations of the motion. In contrast, $\Omega_S^2$ in Fig. 1(e) has large fluctuations at the shortest timescales, indicating large fluctuations of the motion relative to $M^2(\Delta t)$ on those timescales. At larger timescales, the temporal averaging reduces $\Omega_S^2$ toward zero.

As defined, $\Omega_S^2$ is local in space and time. To focus on the space dependence of the fluctuations we need to evaluate a single nondimensional scalar quantity $\Omega(N)$ characterizing the mobility fluctuations for subsystems of size $N$ (the ratio of the dispersion to the average [39] for the particle squared displacements). To do so we partition the system into distinct cubical boxes containing $N$ particles each and evaluate the sum of $\Omega_S^2(t',t'')$ over all time pairs $(t',t'')$ [i.e., the sum over all points in the scatter plot shown in Fig. 1(e)] divided by the number of such pairs for each of the boxes. We then average the resulting number over all boxes and finally take the square root of the result. This procedure yields the desired scalar quantity $\Omega(N)$.

Note that the magnitude of $\Omega(N)$ depends on the total time studied, that is, the maximum of $|t'' - t'|$ that is studied. As is apparent from Figs. 1(c) and 1(e), at large $|t'' - t'|$, $\Omega_S$ decays to zero, and the more of this included in the average, the smaller $\Omega(N)$ will be. However, for a given data set, the magnitude of $\Omega_S$ is unimportant; what matters is the $N$ dependence which is insensitive to the total time studied, as long as that time is sufficient to capture the temporal fluctuations seen in Fig. 1(c). That is, the key point is to include several of the "islands" seen in Figs. 1(a) and 1(c). We have verified that a total duration of $\approx 3\Delta t^*$ gives adequate results for the data we have examined, and $10\Delta t^*$ gives similar results with less noise [where $\Delta t^*$ depends on the temperature (for the Lennard-Jones simulations) or the volume fraction (for the colloidal experiments)]. We use $10\Delta t^*$ for the results we present below to allow for a fair comparison between different data sets.

$\Omega(N)$ for the Lennard-Jones system is plotted in Fig. 2(a), and for the colloidal experiments in Fig. 2(b). In both cases, we see how the dynamical fluctuations average out for larger subsystem sizes. Notably, the systems closer to the glass transition require larger subsystems before the dynamical fluctuations are averaged out—colder systems for the LJ data (a), and higher volume fraction systems for the colloidal data (b).

An interesting point emerges when analyzing the functional form of the decay of $\Omega(N)$ with $N$. From the high-temperature data of Fig. 2(a) we observe the spatially localized dynamic fluctuations measured by $\Omega$ display the usual $N^{-1/2}$ size scaling dependence. This reflects that particle motion is nearly spatially uncorrelated within a subsystem and so the average of $\Delta^2(N)$ converges to the large-system limit $M^2$ as $N^{-1/2}$. However, for glassier systems a clear departure from this trivial behavior is seen, and the decay of $\Omega(N)$ gets slower. The fact that the localized dynamical fluctuations are higher than expected, persisting at large system sizes, speaks of the existence of regions of correlated mobile particles, an effect that is more pronounced upon supercooling [12,15–17,25,32]. We truncate our calculation at $N = N_{\max}/10$, as we desire at least ten subsystems to evaluate a reasonable $\Omega(N)$. We note that for both the Lennard-Jones system and the colloidal suspensions, the behavior of the curves of Figs. 2(a) and 2(b) at very large system sizes is due to lack of statistics (the subsystems are not small as compared to the large system and, thus, we can only average over a few of them). The decay of the curves in Figs. 2(a) and 2(b) presents a notable difference between our approach and that of Refs. [37,38]. The prior work studied how $\chi_4$, a measure of dynamical fluctuations, approached an asymptotic limit as the subsystem size was increased. A critical length scale was identified by the subsystem size needed to reach this asymptotic limit, which required a scaling collapse in Ref. [38]. In contrast, rather than approaching an asymptote, our method approaches zero as the subsystem size increases, enabling us to see subtle differences from the full system behavior. Moreover, our approach does not require any particular scaling collapse, and indeed the power-law behavior seen in Fig. 2(a) may well be something different for different quantities or different systems.

As evident from Figs. 2(a) and 2(b), for the smallest possible subsystems ($N = 1$), the increasing value of $\Omega$ as the glass transition is approached reflects the well-known increasing non-Gaussian nature of the displacement distribution [31]. In fact, this points out a limitation of $\Omega$, in that large values of $\Omega$ can reflect either spatial fluctuations in the dynamics or simply a non-Gaussian distribution of displacements. To remove the latter influence (i.e., to remove the trivial system size dependence and thus to highlight the local correlations) we separately

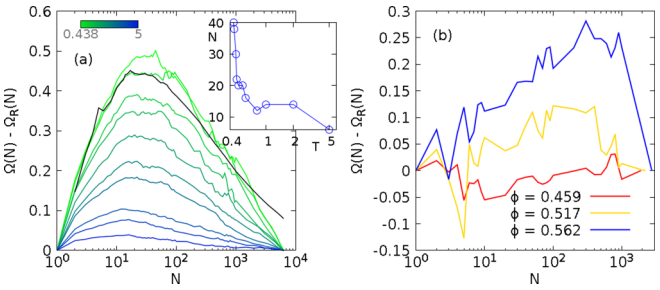


FIG. 3. Subtracting Ω calculated for randomly chosen particles from Ω calculated for compact subsystems. (a) For the LJ system. The inset shows the maximum of the curves as a function of temperature. (b) The same quantity for the colloidal suspensions. The black curve in (a) shows the same quantity evaluated for a system of $10^6$ particles at $T = 0.466$, showing that the position of the maximum is not affected by the finite size of the investigated system.

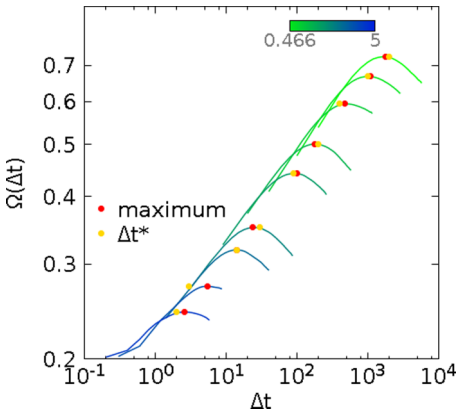


FIG. 4. $\Omega(\Delta t)$ averaged over all subsystem sizes $N$, for the LJ data with different temperatures as indicated by the color scale. Red circles indicate the peak of each curve, and yellow circles indicate the timescale $\Delta t^*$.

compute $\Omega_R(N)$ based not on compact subsystems of size $N$ but on $N$ randomly chosen particles. Here the subscript $R$ indicates an average over many such randomly chosen subsets. For the Lennard-Jones system, this is plotted in Fig. 2(c), showing different behavior from Fig. 2(a) for the colder temperature data. In fact, now the randomly distributed dynamical fluctuations quantified by $\Omega_R(S)$ display the typical $N^{-1/2}$ decay at all temperatures. Similar behavior is found in Fig. 2(d) for the colloidal suspensions, as compared to Fig. 2(b). Again, the $N^{-1/2}$ scaling is recovered at all volume fractions.

To understand the differences between the spatially localized and the randomly distributed dynamic fluctuations, in Fig. 3(a) we show the result of subtracting $\Omega_R(N)$ from $\Omega(N)$. For $N = 1$ particles the result is zero as there is no distinction between the two calculations. Likewise for $N \to 6400$ (the total number of $A$ particles), the two calculations are identical. At intermediate numbers of particles, nonzero values are found in Fig. 3(a) indicating nontrivial spatially localized values of Ω. In particular, for colder temperatures the dynamical fluctuations are larger [higher curves in Fig. 3(a)] and the subsystem size with the largest fluctuations grows slightly [peak position shifts rightward in Fig. 3(a)]. This last observation is quantified in the inset of Fig. 3(a) which shows the peak position of the curves as a function of $T$. The peak occurs for larger subsystems at colder temperatures. This indicates the size of regions with maximally variable dynamics contain about 50 particles for the coldest samples. This leads to a length scale for these dynamical fluctuations of $\sigma N_{\max}^{1/3} = 3.7\sigma$ in terms of the particle diameter $\sigma$. For hotter samples, the maximum shifts to smaller system sizes; for the hottest data, Ω for compact subsystems is nearly indistinguishable from Ω calculated for random particles, and we cannot identify a maximum. In turn, Fig. 3(b) shows the behavior for the colloidal suspensions, which is similar to that found for the Lennard-Jones system. Namely, there is a peak in Fig. 3(b) at a specific subsystem size, and the position and height of this peak is larger for volume fractions closer to the glass transition volume fraction ($\phi_g \approx 0.58$ [32]). An intriguing difference is that the peak position indicates that larger subsystems containing a few hundred particles are maximally heterogeneous, as compared to Fig. 3(a) which peaks at subsystem sizes containing a few tens of particles. We note that these estimates for the length scales all are based on compact subregions (like that found in [28,29]), while this need not be always the case.

Earlier work with the Lennard-Jones system found mobile clusters containing 10–30 particles [40] or 40 particles [28] at the coldest temperatures, in agreement with our result. Likewise, earlier analyses of the same colloidal data found the largest mobile clusters contained ∼50 particles on average for $\phi = 0.562$ [32]. The new result seen here is how the sample behaves over larger length scales. For example, Fig. 3(a) shows that there is still nontrivial spatial heterogeneity for subsystems containing $N = 1000$ particles, more than an order of magnitude larger than the $N$ corresponding to the peak. This is strong evidence that the dynamically heterogeneous regions of size $N \sim 50$ are not randomly distributed throughout the sample but are themselves spatially clustered, over length scales up to and beyond $\sigma N^{1/3} = 10\sigma$.

In this analysis, $\Omega_S^2$ is averaged over timescales to highlight the $N$ dependence of the dynamical fluctuations. We now turn to the complementary case, and average $\Omega_S^2$ over subsystem sizes $N$ to single out the timescale $\Delta t$ of the same fluctuations. Since the value of $N$ covers several orders of magnitude, we average $\Omega_S(t',t'')$ over subsystems with sizes $N$ picked to be evenly distributed in $\log(N)$, with $N$ ranging from 1 to the system size. We first average over all subsystems of a given size $N$, and then average $\Omega^2(N,t',t'')$ over $N$ and $(t',t'')$ with fixed time interval $\Delta t = t'' - t'$ to result in $\Omega(\Delta t)$. This is shown in Fig. 4 where the peak of each curve is marked with a red circle. For comparison, the timescale $\Delta t^*$ is indicated for each data set with a yellow circle; it appears the peak of $\Omega(\Delta t)$ is always close to the non-Gaussian timescale $\Delta t^*$. As expected, the timescale of maximum dynamical heterogeneity [as measured by $\Omega(\Delta t)$] grows as the system approaches the glass transition. Of course, other measures of dynamical heterogeneity can peak at other timescales [30]. We note that our method can be generalized to treat other quantities besides displacements, and so the peak timescale may well vary with other examined quantities.

In summary, we have constructed a measure of spatial and temporal dynamic heterogeneity. The measure does not require defining subsets of mobile or immobile particles, but rather

looks for fluctuations away from the large system behavior. Additionally, it allows us to examine dynamical heterogeneity on a variety of length scales, showing that the approach to the large system limit is slower than would be expected for randomly distributed fluctuations in the dynamics. That is, not only are there relatively mobile and immobile regions within the sample as has been long known, but also there are subtle spatial correlations between these regions that persist over long length scales. The method can be straightforwardly applied to experimental systems such as the dense colloidal solution we examine; it does not require finite-size scaling, for example. While we focus on particle motion where the mean-square displacement is the null hypothesis, the method can be generalized to any other spatially and temporally fluctuating quantities, as long as there is a well-defined null hypothesis based on the large system limit.

The work of E.R.W. was supported by a grant from the National Science Foundation (Grant No. DMR-1609763). G.A.A. and J.A.R.F. acknowledge support from CONICET (PIP2015-2017), UNS (PGI-24/Q062), and ANPCyT (PICT2015/1893). We are grateful to Prof. Walter Kob for past conversations.

[1] C. A. Angell, Science **267**, 1924 (1995).
[2] C. A. Angell, K. L. Ngai, G. B. McKenna, P. F. McMillan, and S. W. Martin, J. Appl. Phys. **88**, 3113 (2000).
[3] J. S. Langer, Rep. Prog. Phys. **77**, 042501 (2014).
[4] D. Chandler and J. P. Garrahan, Ann. Rev. Phys. Chem. **61**, 191 (2010).
[5] G. Biroli and J. P. Garrahan, J. Chem. Phys. **138**, 12A301 (2013).
[6] M. D. Ediger and P. Harrowell, J. Chem. Phys. **137**, 080901 (2012).
[7] V. Lubchenko and P. G. Wolynes, Ann. Rev. Phys. Chem. **58**, 235 (2007).
[8] A. Cavagna, Phys. Rep. **476**, 51 (2009).
[9] P. Charbonneau, J. Kurchan, G. Parisi, P. Urbani, and F. Zamponi, Ann. Rev. Condens. Matter Phys. **8**, 265 (2017).
[10] H. Sillescu, J. Non-Cryst. Solids **243**, 81 (1999).
[11] M. D. Ediger, Ann. Rev. Phys. Chem. **51**, 99 (2000).
[12] S. C. Glotzer, J. Non-Cryst. Solids **274**, 342 (2000).
[13] E. Hempel, G. Hempel, A. Hensel, C. Schick, and E. Donth, J. Phys. Chem. B **104**, 2460 (2000).
[14] R. Richert, J. Phys.: Condens. Matter **14**, R703 (2002).
[15] W. Kob, C. Donati, S. J. Plimpton, P. H. Poole, and S. C. Glotzer, Phys. Rev. Lett. **79**, 2827 (1997).
[16] C. Donati, J. F. Douglas, W. Kob, S. J. Plimpton, P. H. Poole, and S. C. Glotzer, Phys. Rev. Lett. **80**, 2338 (1998).
[17] C. Donati, S. C. Glotzer, and P. H. Poole, Phys. Rev. Lett. **82**, 5064 (1999).
[18] J. P. Garrahan and D. Chandler, Proc. Natl. Acad. Sci. USA **100**, 9710 (2003).
[19] A. S. Keys, L. O. Hedges, J. P. Garrahan, S. C. Glotzer, and D. Chandler, Phys. Rev. X **1**, 021013 (2011).
[20] A. Rahman, Phys. Rev. **136**, A405 (1964).
[21] M. M. Hurley and P. Harrowell, Phys. Rev. E **52**, 1694 (1995).
[22] M. M. Hurley and P. Harrowell, J. Chem. Phys. **105**, 10521 (1996).
[23] E. Flenner and G. Szamel, J. Phys.: Condens. Matter **19**, 205125 (2007).
[24] B. Doliwa and A. Heuer, Phys. Rev. E **61**, 6898 (2000).
[25] E. R. Weeks, J. C. Crocker, and D. A. Weitz, J. Phys.: Condens. Matter **19**, 205131 (2007).
[26] N. Lačević, F. W. Starr, T. B. Schrøder, and S. C. Glotzer, J. Chem. Phys. **119**, 7372 (2003).
[27] A. S. Keys, A. R. Abate, S. C. Glotzer, and D. J. Durian, Nat. Phys. **3**, 260 (2007).
[28] G. A. Appignanesi, J. A. Rodriguez Fris, R. A. Montani, and W. Kob, Phys. Rev. Lett. **96**, 057801 (2006).
[29] G. A. Appignanesi and J. A. Rodriguez Fris, J. Phys.: Condens. Matter **21**, 203103 (2009).
[30] C. Toninelli, M. Wyart, L. Berthier, G. Biroli, and J.-P. Bouchaud, Phys. Rev. E **71**, 041505 (2005).
[31] W. Kob and H. C. Andersen, Phys. Rev. E **51**, 4626 (1995).
[32] E. R. Weeks, J. C. Crocker, A. C. Levitt, A. Schofield, and D. A. Weitz, Science **287**, 627 (2000).
[33] C. P. Royall and S. R. Williams, Phys. Rep. **560**, 1 (2015).
[34] C. P. Royall, S. R. Williams, T. Ohtsuka, and H. Tanaka, Nat. Mater. **7**, 556 (2008).
[35] I. Ohmine and H. Tanaka, Chem. Rev. **93**, 2545 (1993).
[36] E. La Nave and F. Sciortino, J. Phys. Chem. B **108**, 19663 (2004).
[37] K. E. Avila, H. E. Castillo, A. Fiege, K. Vollmayr-Lee, and A. Zippelius, Phys. Rev. Lett. **113**, 025701 (2014).
[38] S. Chakrabarty, I. Tah, S. Karmakar, and C. Dasgupta, Phys. Rev. Lett. **119**, 205502 (2017).
[39] D. Chandler, in *Introduction to Modern Statistical Mechanics*, (Oxford University Press, New York, 1987), p. 288.
[40] C. Donati, S. C. Glotzer, P. H. Poole, W. Kob, and S. J. Plimpton, Phys. Rev. E **60**, 3107 (1999).